water

MDPI

Groundwater Vulnerability and Potentially Toxic Elements Associated with the Iron Mining District of Ouixane (Northeast of Morocco)

Azzeddine Khafouri [1], **El Hassan Talbi** [1], **Abdessalam Abdelouas** [2], **Khalid Benjmel** [3], **Isabel Margarida Horta Ribeiro Antunes** [4] **and Mohamed Abioui** [5,6,*]

1   Laboratory of Geoheritage, Geoenvironment and Prospecting of Mines & Water, Department of Earth Sciences, Faculty of Sciences, Mohammed Premier University, Oujda 60000, Morocco
2   SUBATECH Department, UMR CNRS 6457, IMT Atlantique, University of Nantes, BP 20722, CEDEX 3, 44307 Nantes, France
3   Laboratory of Geosciences Applied to Engineering Development (GAIA), Faculty of Science Ain-Chock, Hassan II University of Casablanca, Maarif, Casablanca 20150, Morocco
4   Institute of Earth Sciences, Pole of University of Minho, 4710-057 Braga, Portugal
5   Department of Earth Sciences, Faculty of Sciences, Ibn Zohr University, Agadir 80000, Morocco
6   MARE-Marine and Environmental Sciences Centre—Sedimentary Geology Group, Department of Earth Sciences, Faculty of Sciences and Technology, University of Coimbra, 3030-790 Coimbra, Portugal
*   Correspondence: m.abioui@uiz.ac.ma

Abstract: This study aims to investigate the groundwater vulnerability concerning potentially toxic elements in the vicinity of the abandoned iron mine of Ouixane (Morocco). A modified DRASTIC method (DRSTI) is proposed with satisfactory results. High vulnerability zones represent 40% of the study area, while medium and low vulnerability represent, respectively, 42% and 18% of the study area. These results have been validated by groundwater geochemical analyses of potentially toxic elements carried out in the framework of previous studies in the same area. Thus, the superposition of the waste rock and tailings map with the vulnerability map showed that the latter is located in areas of high to medium vulnerability and therefore constitutes the main cause of the deterioration of the geochemical quality of groundwater. Otherwise, the vulnerability method showed that the main parameters that significantly affect the vulnerability are: the depth of water (D), net recharge (R), and the unsaturated zone (I), while the other parameters do not significantly affect the model used and do not have much influence on the results of the vulnerability assessment. The method used allowed us to locate the most vulnerable areas to potentially metallic toxic elements pollution resulting from the abandoned iron mine of Ouixane, and it constitutes a tool for decision support and for developing effective action plans to mitigate and monitor the effects of the transfer of potentially toxic elements pollution to groundwater.

Keywords: vulnerability; DRSTI; groundwater; metallic pollution; mining district; Ouixane mine

1. Introduction

The contamination of water resources in the vicinity of mining sites is an international problem, especially in emerging countries that do not have specific regulations and a legal framework for environmental protection and preservation, throughout the exploitation period and after closing and restoration.

Groundwater is the most important water source for supplying arid and semi-arid regions. In these climatic areas, groundwater has large volumes and a low vulnerability to pollution when compared to surface waters [1]. Several studies have focused on the environmental pollution of the mining sites, particularly with potentially toxic elements, and the impact of the mining industry, especially on surface and groundwater resources. Most of these studies have shown that potentially toxic elements pollution can irreversibly

affect the ecosystem in the absence of adequate protection measures [2]. Pollutants from mining and related activities can be mobilized and transferred to contaminate liquid and solid environmental compartments [3].

The deposits of the Ouixane iron mining district are located on the Beni Bou Ifrour massif, 10 km southwest of Nador city (northeast of Morocco). The three famous deposits are: Ouixane, Axara-Imnassen, and Bokoya-Setolazar distributed on a rugged topography and spread over an area of 36 km^2.

The Ouixane iron deposits were discovered by the Spanish geologist A. DelVall at the beginning of the 20th century, and the area was exploited from 1914 onwards by the Spanish company CEMR (Spanish Rif Mining Company) until the Moroccan government took over the management of the site. The mine has produced more than 65 million tons of iron ore, mainly hematite and magnetite, with a volume of 1.5 million m^3/year of waste rock of various natures and during different stages of extraction. The existence of sulfide-laden ores (pyrite, pyrrhotite, and chalcopyrite) exposed directly to climatic conditions (water, air, temperature) promote chemical and microbiological (e.g., *bacterium thiobacillus*) oxidation reactions of the tailings. The main reaction includes the production of sulfuric acid (H_2SO_4), which leads to a decrease in the water pH and consequently the increase in the mobility and dispersion of potentially toxic elements in the environment. These reactions give rise to the formation of acid mine drainage (AMD).

Most of the research studies carried out previously to characterize the environment of the Ouixane mining district were limited to the geology [4,5] and hydrogeology [6] of the area, the study of iron mineralization [7,8], soil pollution [9], etc. However, no author has developed the problem of transfer of metal pollutants to the water table; only Lakrim [9] developed his method in 2016, but this does not take into account very important parameters in the study of vertical transfer of these toxic pollutants such as the unsaturated zone, the depth of water, the net recharge, and the soil media.

The present study aims to assess the intrinsic vulnerability and groundwater pollution risk associated with potentially toxic elements in the vicinity of the Ouixane iron mining district, northeast of Morocco. Groundwater vulnerability results have been validated by groundwater geochemical analyses associated with potential mining activities, carried out in the framework of previous studies in the area, and by the application of a sensitivity statistical test.

This work provides a vision of the intrinsic vulnerability of groundwater, validated by real analysis data published, and the method is also coupled with the spatial distribution map of tailing and mining waste to identify high-risk areas to facilitate managers and decision-makers to establish a strategy and action plans to intervene, whether in the rehabilitation of the abandoned mine, the depollution and mitigation of the negative effects of mining waste, or to install a system for regular monitoring of the evolution of metallic pollution of the Ouixane groundwater.

The results of this study will help to: (i) identify the parameters causing vulnerability and to intervene in a targeted way on these parameters (control of parameters related to the diffusion of contamination to the groundwater), (ii) guide the decision-makers in the development of action plans with priority to areas characterized as "high-risk", given that the reclamation and mining decontamination costs are expensive for a developing country such as Morocco.

2. Study Area

The study area is a part of the Beni Bou Ifrour massif (Figure 1), which hosts the Ouixane mining district. This mining district contains several deposits that were prospected from 1905 to 1907 and then exploited from 1907 onwards for almost a century [10]. The uncontrolled exploitation has left behind abandoned open pits and underground deposits and millions of tons of waste rock and mining waste on the environment, which could affect water resources, in particular [11,12]. The area is characterized by a semi-arid Mediterranean climate with an annual rainfall of around 200 to 400 mm/year [13].
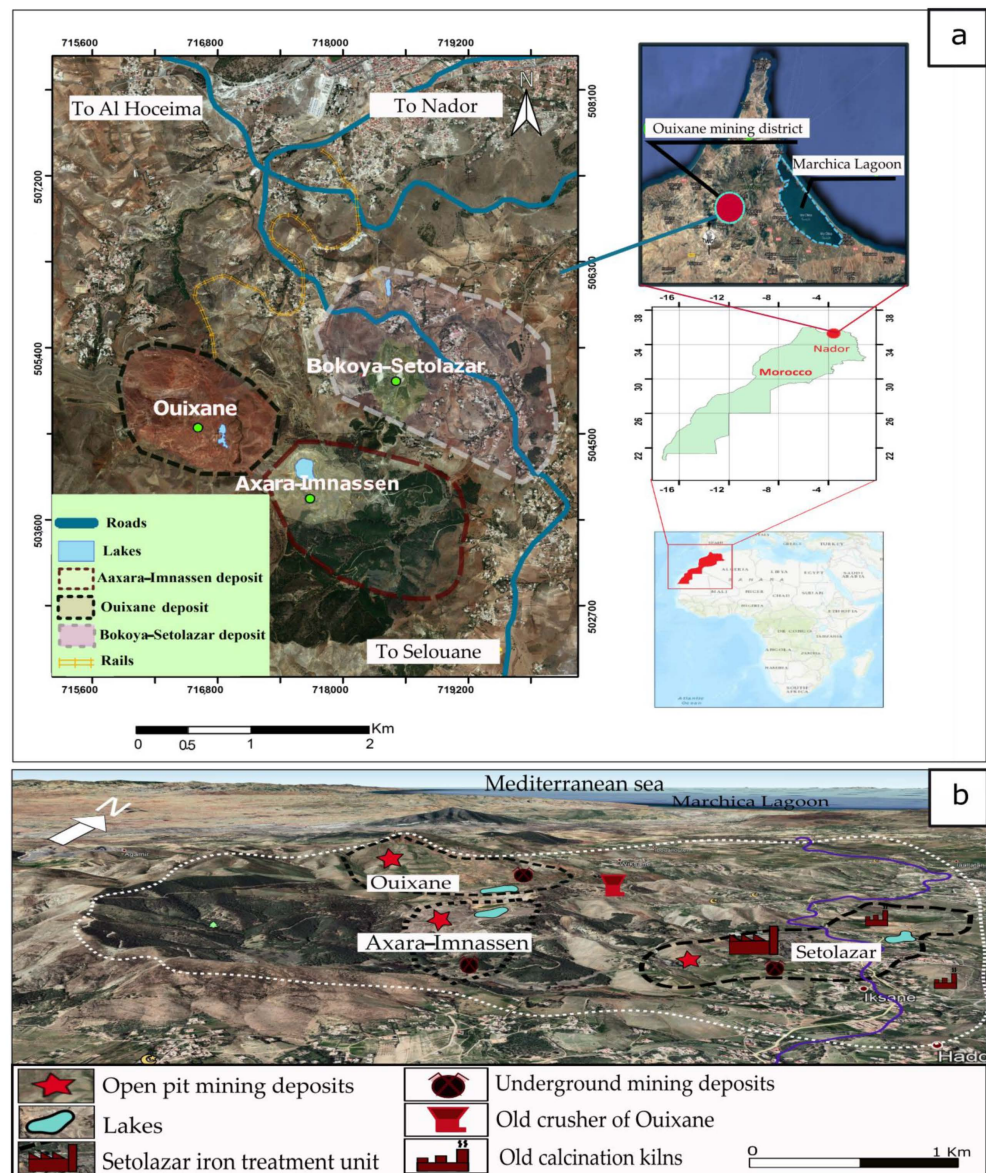
Figure 1. Geographical setting (**a**) and 3D satellite view (**b**) of the Ouixane iron mining district (northeast of Morocco).

The Beni Bou Ifrour deposit is a skarn-type magnetite deposit. The determination of K-Ar age suggests that the mineralization occurred at 7.04 ± 0.47 Ma, and the mineralizations are probably related to the Ouixane granodiorite [7,14].

The massif of Beni Bou Ifrour consists of limestones and silver-bearing shales of the Lias-Neocomian (unit Jebel Harcha), while the Ouixane unit consists of marls, sandstones, and limestones of the Upper Jurassic (Tithonian), and sandstone, schists, and volcano-sedimentary rocks of the Lower Cretaceous (Berriasian). All these units are covered by molasses from the Miocene age [5].

The Ouixane unit is more deformed than the surrounding area, and the fault network is dense (Figure 2) with large faults such as those of Ouixane, Cherif, and Iberkanene. It is the most oxidized zone, and the main iron ore mineralizations correspond to hematite with magnetite and very little sulfide minerals.

The groundwater piezometric level of the unconfined aquifer in the vicinity of the Beni Bou Ifrour massif ranges between 10 and 50 m deep (Figure 3), thus the dominant groundwater flow occurs from southwest to northeast [15,16]. The permeability more

widespread in the study area is approximately 10^{-4} m/s [6], and hydraulic conductivity values increase towards the Nador lagoon, reaching a value of 5×10^{-4} m/s [16].
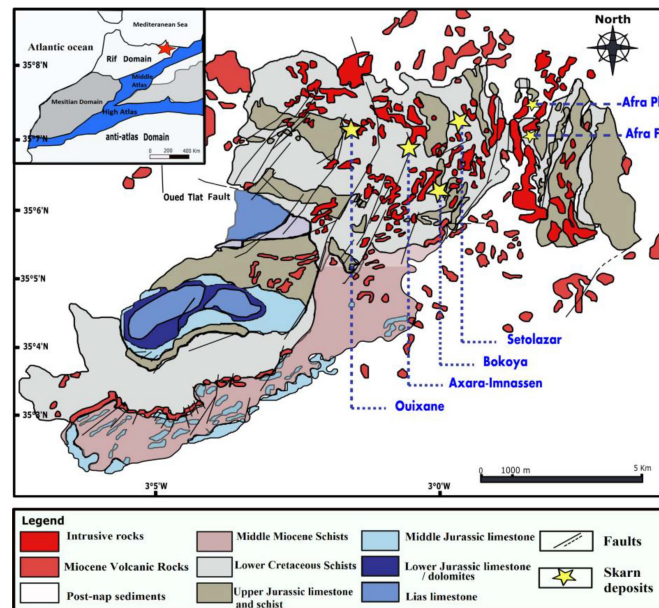

Figure 2. Location of the main Ouixane iron deposits from the mining district on the geological map, modified after [8,14].
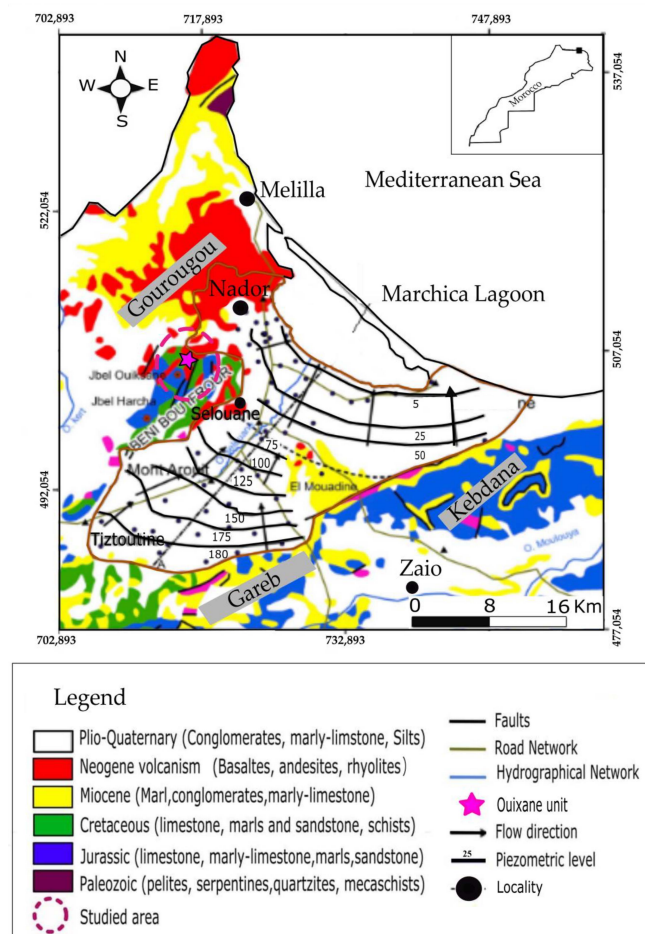

Figure 3. Piezometric and geological map of the study area based on the geological map of Morocco 1/1,000,000. Adapted from [6].

3. Materials and Methods

3.1. Uses of GIS Application

The geographic information system (GIS) tool has been widely used in the storage, management, and analysis of geospatial data and provides decision support for water managers [17]. In this study, GIS was very useful for groundwater vulnerability and risk spatial distribution maps. This application involves the compilation, reprojection, and reclassification of spatial data from various sources and allows for a weighted overlay of different parameters to generate the final vulnerability scores. To carry out this study, ArcGIS 10.2 software was used to develop the assessment score maps by reclassifying each factor data layer and then using the raster calculator to produce the groundwater vulnerability map. The groundwater vulnerability map and mining discharge map are overlayed to obtain a groundwater pollution risk map.

3.2. Groundwater Vulnerability Assessment

This study consists of assessing and mapping groundwater vulnerability in the area around the Ouixane mining district using the modified DRASTIC method [18], a modified version of the classical DRASTIC method, developed by the United States Environmental Protection Agency (US-EPA) in association with the National Water Well Association [19].

On the area was applied a modified DRASTIC vulnerability model—DRSTI—considering five parameters: the depth to an aquifer (D), net recharge (R), soil media (S), topography (T), the impact of the vadose zone (I), and adding the sixth parameter to assess the pollution risk associated to the mining discharges and tailings spatial distribution. The majority of studies did not adequately account for the human factor in their analysis as the other DRASTIC parameters. The influence of land use (LU) on groundwater contamination has been identified as a parameter that receives less attention from most researchers [20].

The DRASTIC method has been used in different studies with different groundwater management, preservation, and sustainability conditions [13,21]. The acronym DRASTIC is derived from the seven parameters that are critical to the transport and attenuation process of contamination. These factors include depth-to-water table (D), recharge (R), aquifer media (A), soil media (S), topography (T), the impact of the vadose zone (I), and hydraulic conductivity of the aquifer (C). Once the different classes have been defined and their scores assigned, the method determines the DRASTIC index (Id), which characterizes the degree of vulnerability of a specific sector of the groundwater surface. The higher the calculated index (Id) is, the greater groundwater vulnerability is associated. This index is defined as follows:

$$Id = (Dr \times Dw) + (Rr \times Rw) + (Ar \times Aw) + (Sr \times Sw) + (Tr \times Tw) + (Ir \times Iw) + (Cr \times Cw) \tag{1}$$

where D, R, A, S, T, I, C represent the defined DRASTIC parameters, and r and w correspond to the weight and score, respectively, assigned to each parameter.

Contrary to the DRASTIC method, which involves parameters relating to the recharge, the unsaturated, and saturated zone of the aquifer, the proposed methodology—modified DRASTIC method (Figure 4)—is based on groundwater recharge, the soil (slope and lithological nature), and the unsaturated zone (nature and thickness). Indeed, only these parameters are considered to be involved in the contaminant transmission from the soil surface to groundwater. Groundwater vulnerability assessment could be studied without considering all the factors of the DRASTIC model such as been considered by different authors [18,22,23], yet this opinion is not shared by others [24,25].
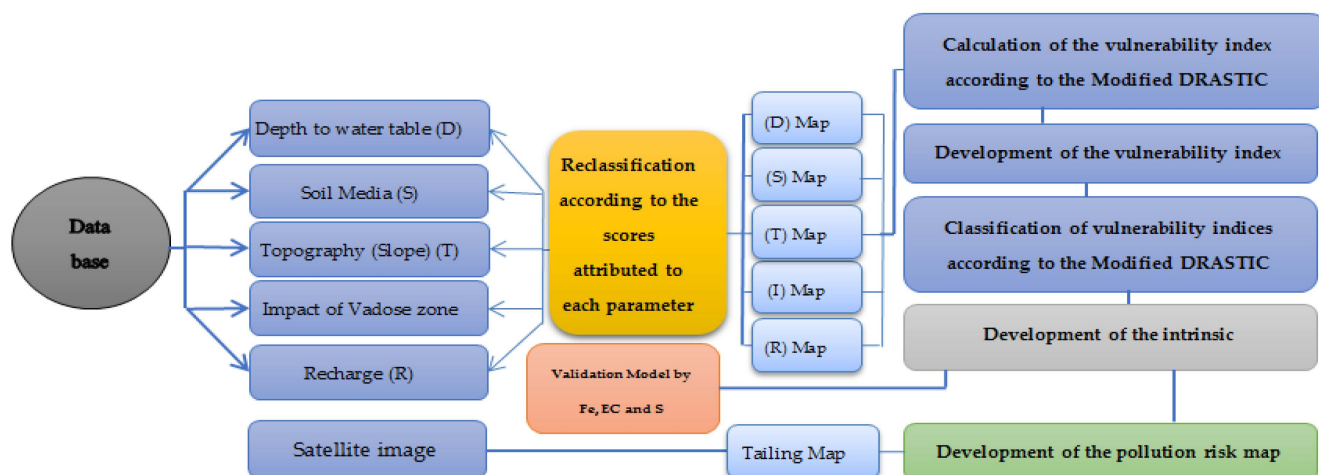
Figure 4. Flow chart of the applied methodology from this study.

The same weights, scores, and classes as those defined by DRASTIC method are assigned to the five parameters used on the new "DRSTI" index. The new vulnerability index (Vi) is calculated according to Equation (2) and Table 1:

$$Vi = (Dr \times Dw) + (Rr \times Rw) + (Sr \times Sw) + (Tr \times Tw) + (Ir \times Iw) \tag{2}$$

Table 1. Rating and weighting values for the vulnerability parameters [19].

Parameters	Range	Score (Rating)	Weight
D (m)	0–1.5	10	5
	1.5–4.5	9	
	4.5–9	7	
	9–15	5	
	15–23	3	
	23–30	2	
	>30	1	
R (mm)	0–50	1	4
	50–100	3	
	100–175	6	
	175–225	8	
	>225	9	
S	None-gravel	10	2
	Sand	9	
	Sandy-loam	6	
	Loam	4	
	Silty-loam	3	
	Clay	1	
T (%)	0–2	10	1
	2–6	9	
	6–12	5	
	12–18	3	
	>18	1	
I	Silt, clay, and shale	2 to 6	5
	Limestone	2 to 5	
	Sandstone	2 to 7	
	Sand, gravel with silt, and clay passage	4 to 8	
	Sand and gravel	4 to 8	
	Basalt	2 to 10	
	Karstic limestone	8 to 10	

The resulting intrinsic vulnerability map from the study area is developed according to the following sequential methodology (Figure 4) and characteristic vulnerability index classification (Table 2).

Table 2. DRSTI vulnerability index classification [19].

Vulnerability Classes	Vulnerability Index
Very low	$27 < Vi \leq 50$
Low	$50 < Vi \leq 80$
Medium	$80 < Vi \leq 110$
High	$110 < Vi \leq 140$
Very high	$140 < Vi \leq 166$

3.3. Development of Groundwater Vulnerability Map and Risk Map

Groundwater vulnerability refers to the potential of a groundwater system to be affected by contamination from the soil surface [26]. The choice of the more appropriate method to assess vulnerability is highly dependent on the objective and scope of a particular study, data availability, and especially, the user's cost and time [27,28]. The risk of contamination is determined both by the intrinsic vulnerability of the aquifer, which is relatively static, and by the existence of potentially polluting mining substances and activities on the soil surface (e.g., treatment unit, crusher, tailings, waste rock, storage dike).

In this study, the land use of the study area is mapped by the different sources that could be a source of potentially toxic elements emission on the surface (e.g., waste rock, tailings). This map will be overlayed with the intrinsic vulnerability map of the studied area to locate the high-risk pollution areas.

3.4. Sensibility Analysis

A sensitivity analysis is essential to identify the most effective vulnerability parameters for planning sustainable aquifer crisis management [29,30]. In addition, it avoids subjectivity and will allow the identification of important and influential model parameters [31,32].

A single-parameter sensitivity measure is developed to evaluate the impact of each of the DRSTI parameters on the groundwater vulnerability index. It allows comparing the "effective" weight with their "theoretical" weight [33], as has been applied in different other studies [27,34,35]. The "effective" weight of each parameter in each subarea is calculated using Equation (3):

$$W_i = (P_{r,i} \times Pw/D_i) \times 100 \tag{3}$$

where W_i refers to the "effective" weight of each parameter $P_{r,i}$ and Pw correspond to the rating value and the weight of each parameter, respectively, while D_i is the overall vulnerability index.

3.5. Model Validation

The validation of the obtained groundwater vulnerability is possible considering obtained physicochemical data, such as Fe concentration and electrical conductivity (EC) values measured from groundwater obtained in the area [3], as well as S groundwater concentrations [9]. The selection of the parameters (Fe, S, and EC) could be justified as the main source of these elements in the groundwater is associated with mining and related activities. Other authors have also used groundwater metal concentration to validate vulnerability models [36,37]. These values are projected directly onto the groundwater vulnerability map.

4. Results and Discussion

4.1. Vulnerability Map

4.1.1. Depth to Water Table (D)

The depth of the water table determines the depth to which a contaminant is transported before reaching the surrounding aquifer media [19,38]. Thus, as the depth of the groundwater level increases, the probability of groundwater attenuation decreases, as deeper groundwater implies longer travel times and less vulnerability to contamination [39]. In the study area, groundwater depth varies between 5 and 50 m [40], corresponding to a score ranging from 3 to 9 (Table 1 and Figure 5).
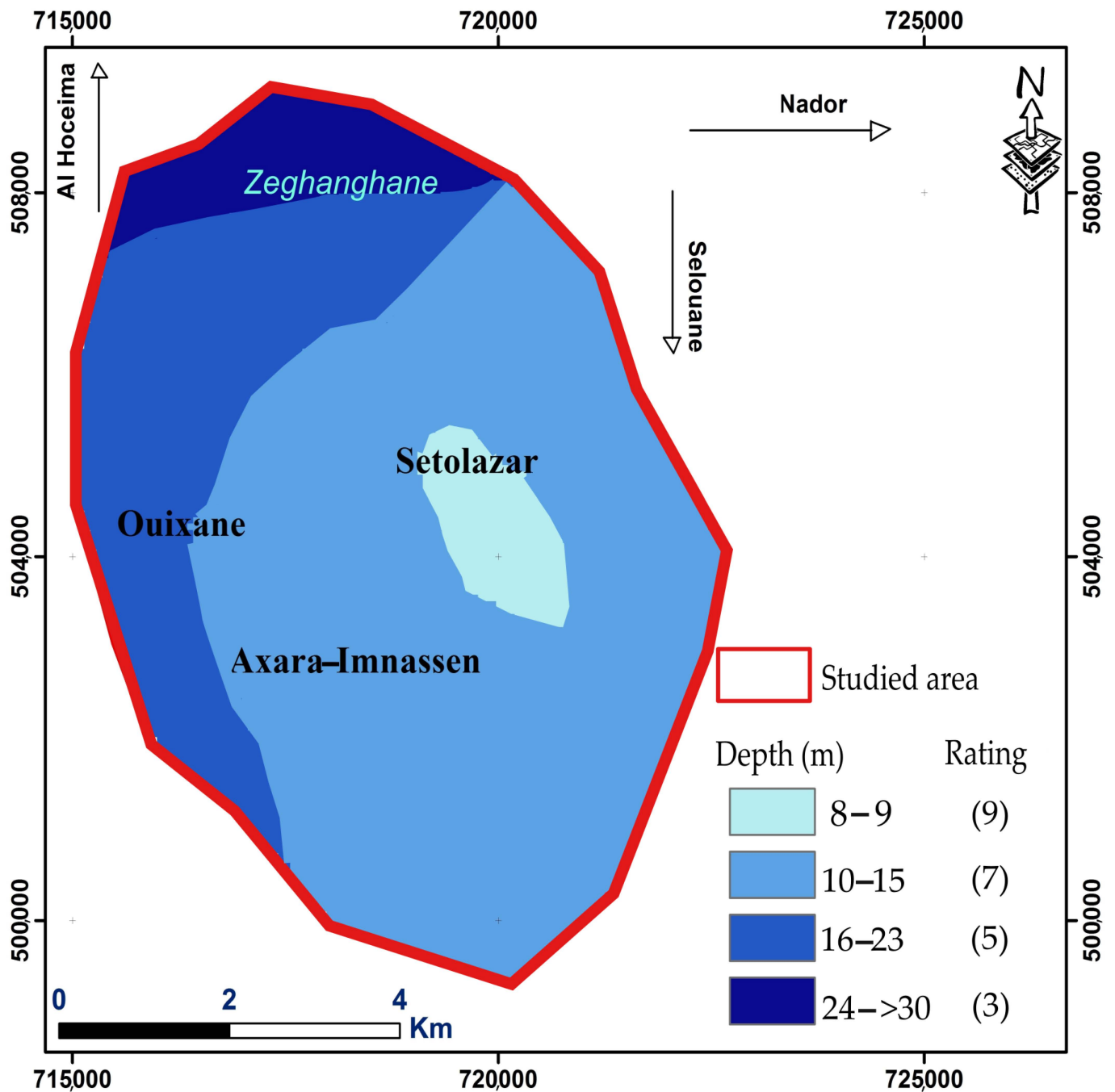

Figure 5. Groundwater depth map and attributed rating values.

4.1.2. Net Recharge (R)

Net recharge is the amount of surface water that could be infiltrated into the soil and reach the groundwater level [41]. This parameter indicates the amount of water from precipitation that is available for vertical transport, dispersion, and dilution of pollutants from a specific application point [19]. The recharged water serves as a carrier for contaminants transportation from the soil and the vadose zone to the aquifer. A higher recharge will allow for more groundwater vulnerability. Annual rainfall data was obtained from the Hydraulic Agency of the Moulouya Basin, with an annual rainfall ranging from 200 to 400 mm/year [40].

The net recharge was calculated based on the Chaturvedi model [42], according to Equation (4):

$$R = 6.75 \, (P - 14)^{0.5} \tag{4}$$

where R is the net recharge and P is the average rainfall (mm/year).

The net recharge map of the study area is classified into two classes and the corresponding scores vary between 8 and 9 (Figure 6).
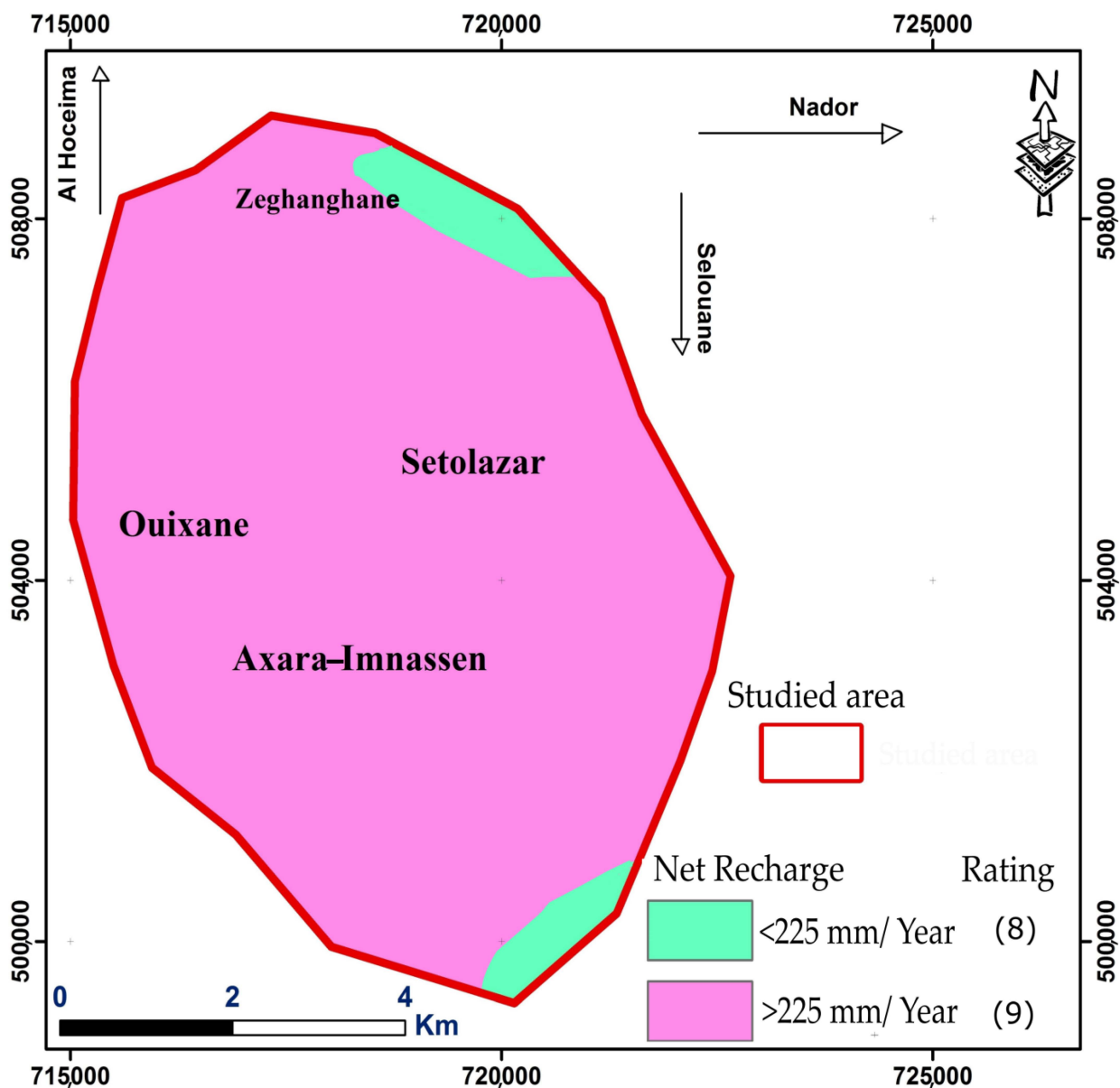

Figure 6. Net recharge map and attributed rating values.

4.1.3. Soil Media (S)

The soil media represents the capabilities of soil to infiltrate water and contaminants vertically from the soil surface to the unsaturated zone. This is based on the permeable character of the soil, which is inherited from the parent rock and compounds [43]. The pedological data were collected from the pedological maps of the Oriental Regional Direction of Agriculture. Soils with clay and silt particles increase the travel time of pollutants. As more grains are larger, the infiltration speed of water and contaminants increases toward the bottom. The main soils in the study area are clay soils, silty clay soils, silty sand soils, gravels and sands, non-fissured clays, and clays and aggregates. Five classes are assigned for the different soil types with a score ranging from 1 to 9 (Figure 7).
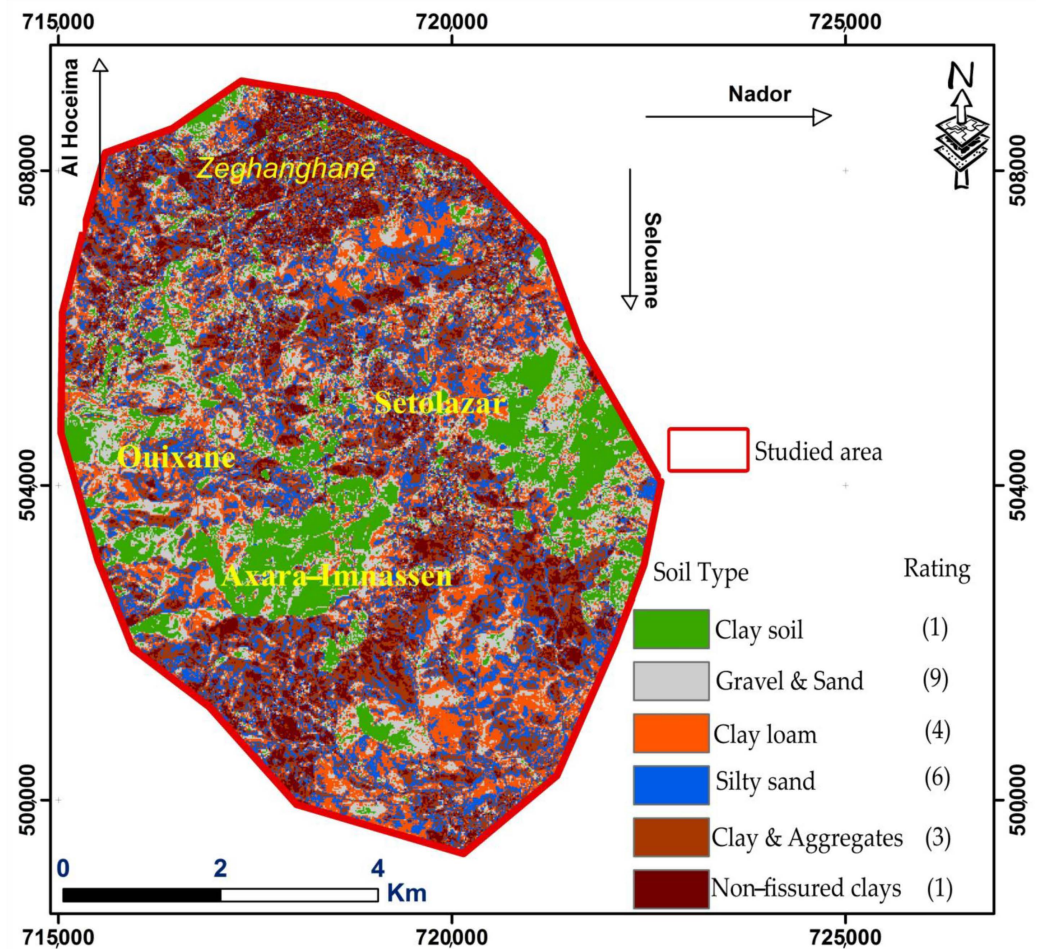

Figure 7. Soil type map and attributed rating values.

4.1.4. Topography (T)

Topography refers to the slope of an area, which determines the runoff and infiltration capacity of the surface water into the soil and consequently the capacity to introduce pollutants into the soil [19,44]. The gentler the slope is (<3%), the higher the retaining capacity of water and/or pollutants, while the steeper the slope is (>18%), the lower the retention capacity of water and/or pollutant [45].

Most of the slopes are gentle; however, they are stronger in the vicinity of the deposits, favoring the transport of metals from the abandoned tailings and waste rock on site to natural and anthropogenic depressions (Figure 8).
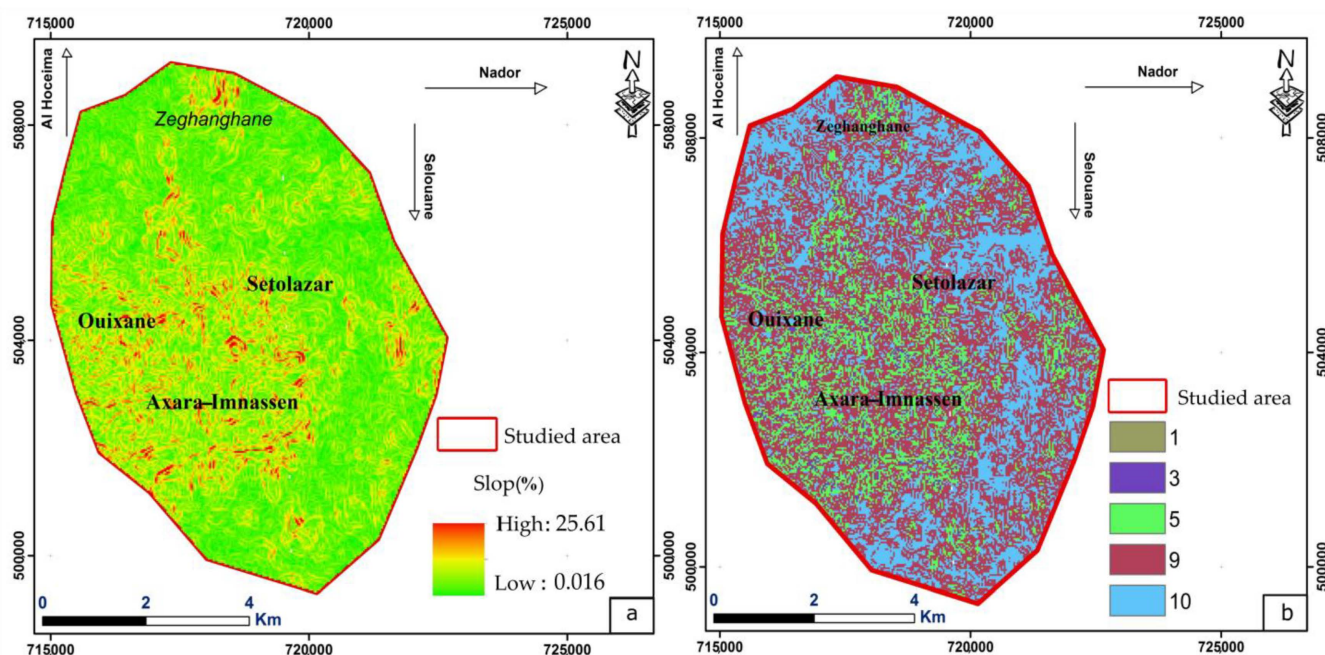
Figure 8. (**a**) Slope map (%) allowing the distinction of the classes of slope indicated in (**b**).

4.1.5. Impact of the Vadose Zone (I)

The vadose zone corresponds to the unsaturated zone materials located below the soil horizon and above the groundwater level. It determines the attenuation characteristics of contaminants [19,46] and controls the contaminant movement to the saturated zone. A vadose zone with high clay content will present a lower pollution potential, whereas, with an increase in the concentration of silt and sand, the pollution potential of the vadose zone increases [47].

The vadose zone from the studied area is composed mainly of conglomerates, igneous, and metamorphic rocks in different stages of alteration, sands, and gravels, lacustrine limestones, clay loams, and schists. The characteristics of soil texture confer the classification into 7 classes, with a score ranging from 2 to 9 (Table 1 and Figure 9).

4.1.6. Groundwater Vulnerability Index Map (Vi)

All thematic maps (or layers) of the parameters used were evaluated according to their importance and susceptibility to contaminants. These layers were multiplied by their weights (Table 1), which were assigned to them according to their importance and contribution to contamination [19,48]. The vulnerability index was calculated by summing the product of each parameter using Equation (2).

The higher the vulnerability index value is, the higher the vulnerability of the aquifer to pollution [32,49,50]. According to the result shown in Figure 10a, the groundwater vulnerability index values of the study area range from 64 to 144.
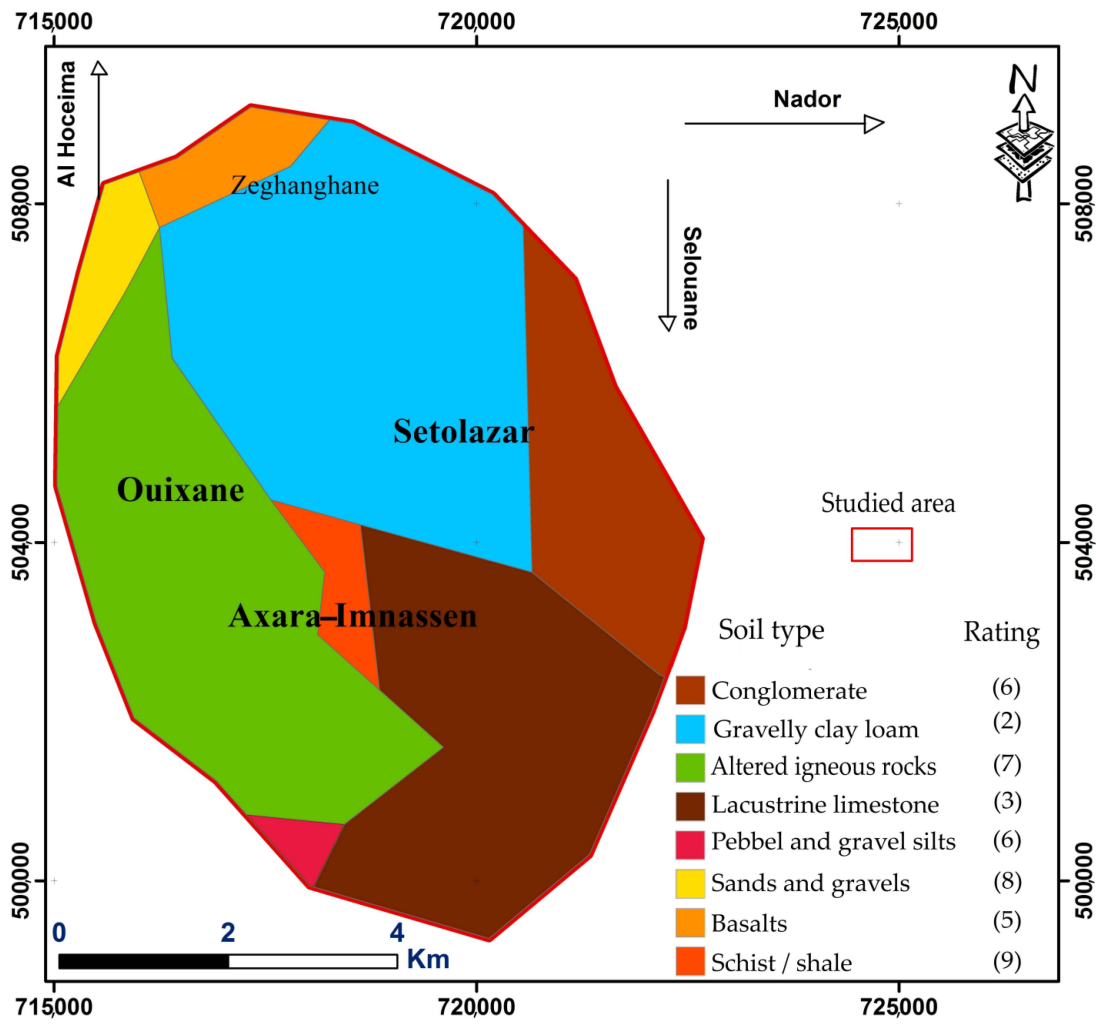
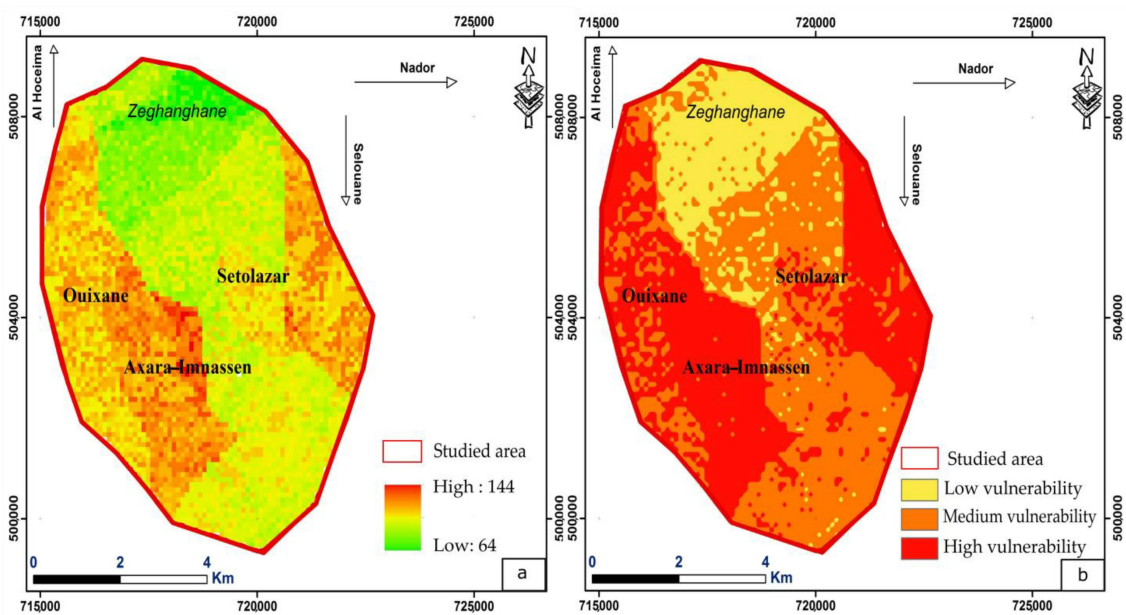**Figure 9.** Vadose zone map (unsaturated zone) and attributed rating values.

Figure 10. (**a**) Vulnerability index map. (**b**) Intrinsic vulnerability map of the studied area.

4.1.7. Groundwater Vulnerability

Vulnerability index values vary between 64–144 (Figure 10a) and are distributed into three classes: low, medium, and high vulnerability (Figure 10b). The analysis of the obtained spatial vulnerability distribution shows a dominance of the "Medium vulnerability" class with a covered area of 42% (i.e., 15 km^2), followed by the "High vulnerability" class, which covers 40% (i.e., 14.5 21 km^2) of the total surface of the study area, while the "Low vulnerability" class is detected in only 18% (i.e., 6.5 km^2) of the total surface area (Figure 11).The areas marked by high and medium vulnerability host the deposits, processing structures, and tailings of the Ouixane mining district (Figure 12).
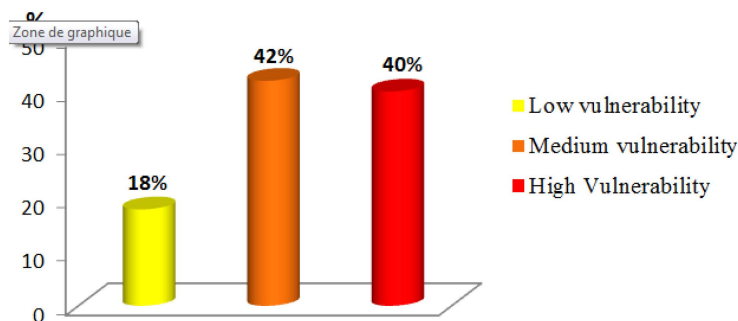

Figure 11. Percentage of the different vulnerability classes in the studied area.
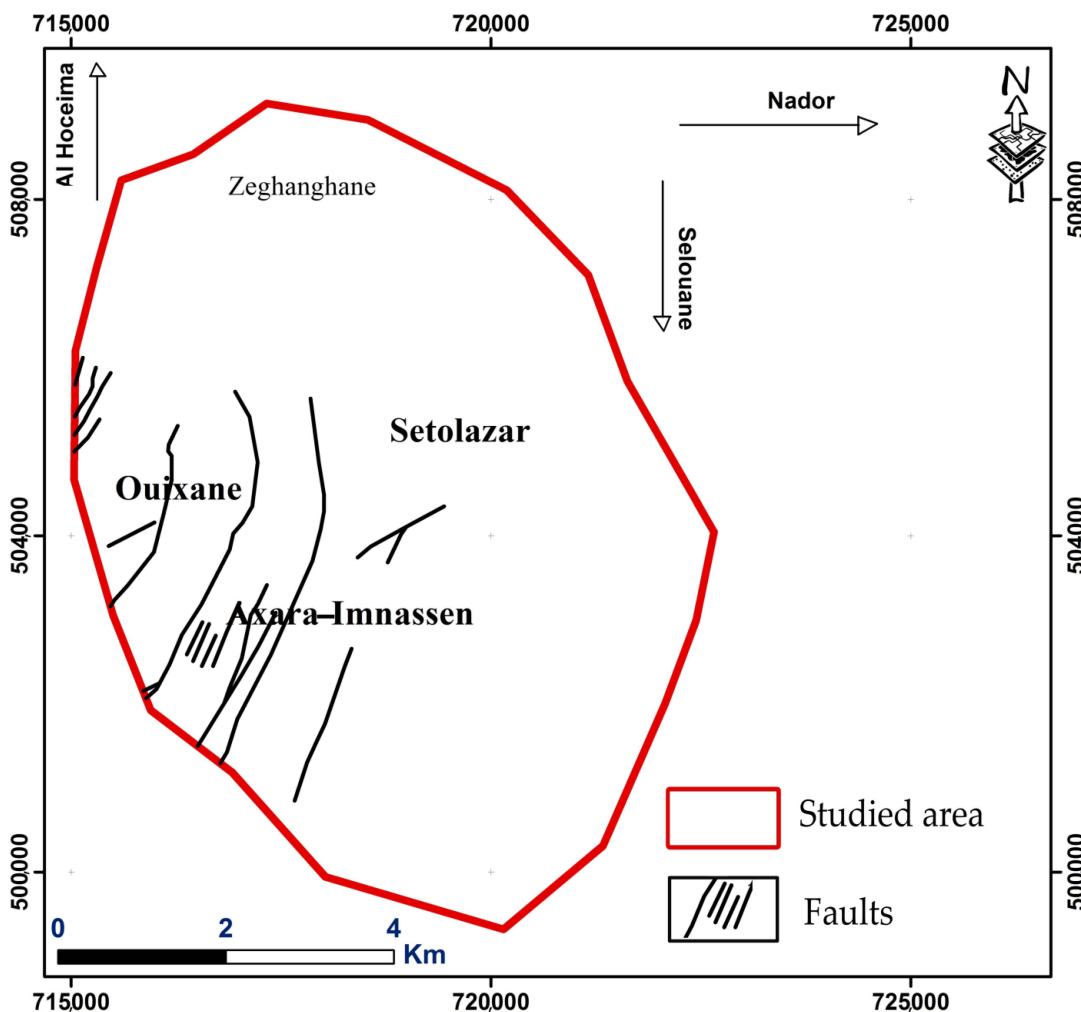

Figure 12. Main geologic faults crossing the iron mining district of Ouixane.

4.1.8. Model Validation and Sensitivity Analysis

To validate the vulnerability areas, the measured (Fe) concentration and groundwater electrical conductivity (EC) from the study area [3], as well as (S) groundwater concentration values [9] were applied. These values are projected directly on the groundwater vulnerability (Figures 13 and 14).
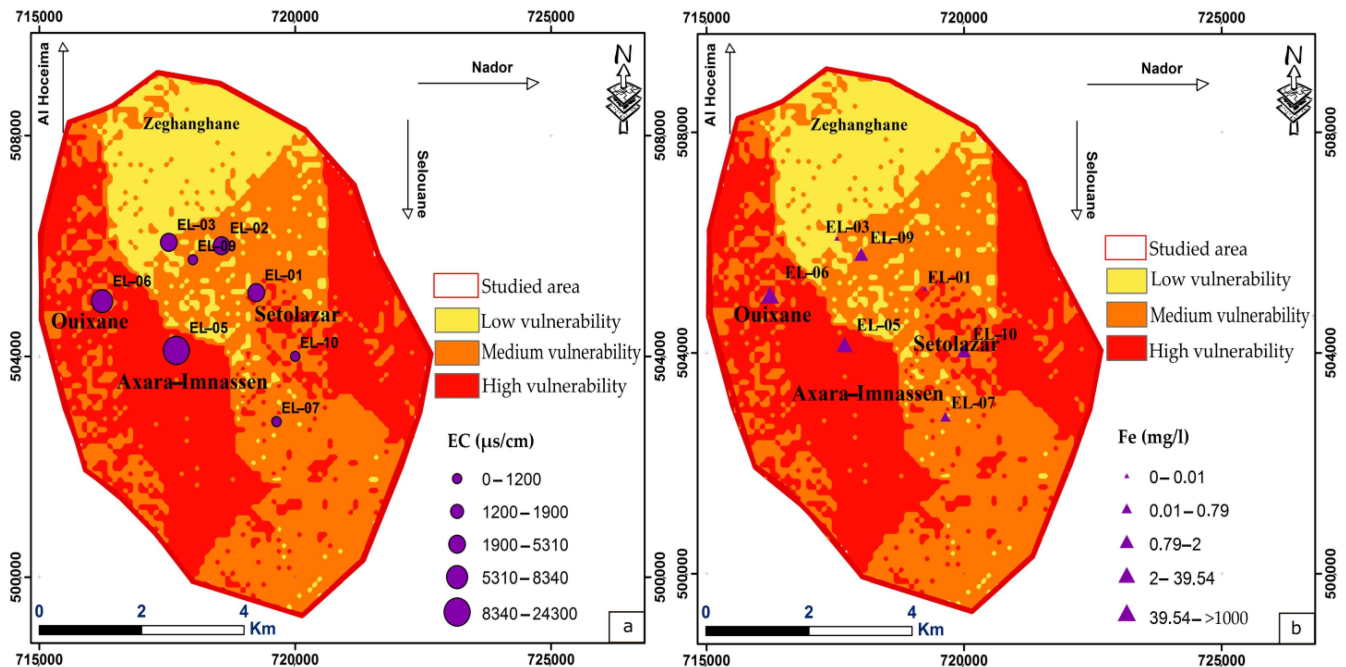

Figure 13. Spatial distribution of groundwater electrical conductivity values (EC) (**a**) and Fe concentrations (mg/L) (**b**), overlaying groundwater vulnerability map of the iron mining district of Ouixane.

The spatial distribution of groundwater iron concentration and electrical conductivity (EC) showed that the highest values of Fe (39.54 to >1000 mg/L) and EC (5310 to 24,300 μs/cm) are observed in the areas with high to medium vulnerability, except for sites EL01, EL09, EL07, and EL10, which presented values of less than 2 mg/Lin Fe, and sites EL09, EL07, and EL10, which presented EC values less than 1200 μs/cm (Figure 13).

Otherwise, the spatial groundwater sulphate concentration distribution overlayed with the groundwater vulnerability map showed that in the medium to high vulnerability areas, especially in the vicinity of the Ouixane, Setolazar, and Axara deposits, the sulphate concentration is higher and varies from 1881.42 to 77,825.43 mg/L (Figure 14).

From the vulnerability map, it can be deduced that groundwater Fe, S, and other metallic elements contamination that will promote groundwater electrical conductivity increase is mainly related to the anthropic effect associated with the Ouixane mineralized deposits exploitation and the uncontrolled storage of waste rock and tailings; favoring the generation of mine drainage and the transfer of metallic pollution flows to the neighboring compartments (e.g., soil, water, plants).

The parameters that play a decisive role in increasing groundwater vulnerability (Table 3) are the depth of water (D), which varies between 10 and 23 m deep, and the unsaturated zone (I), marked by the presence of metamorphic formations and altered igneous rocks and by the presence of an important fault network (Figure 12). Furthermore, the net recharge (R) associated with the precipitation that drains the Ouixane mining district, will promote the dispersion of potentially toxic elements to groundwater depth. The other applied parameters could be considered not significantly involved in the used model and will not have a relevant influence on groundwater vulnerability results.
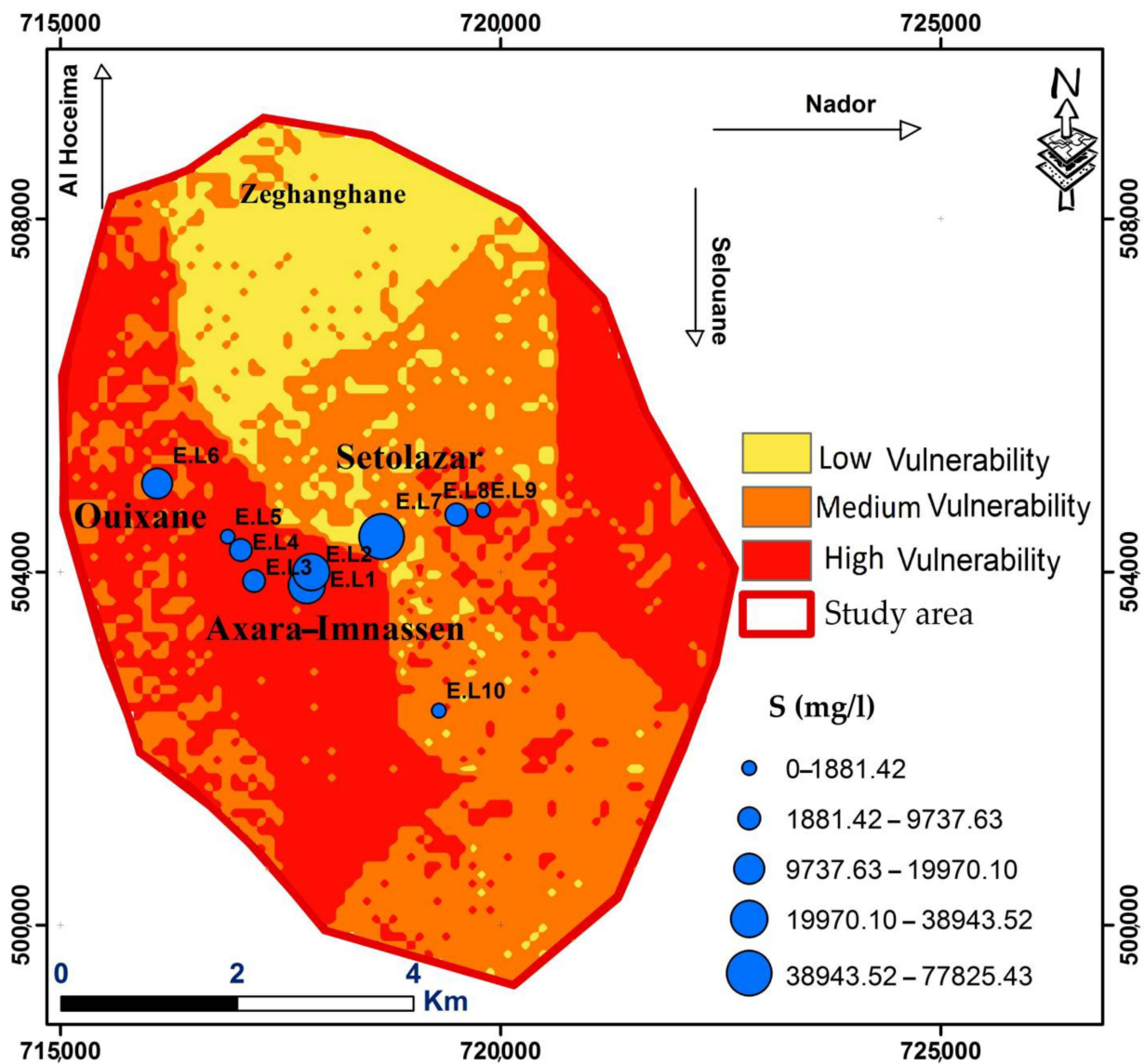
Figure 14. Spatial distribution of groundwater sulfur concentrations on the groundwater vulnerability map of the Ouixane mining district.

Table 3. Statistical analysis results of the single parameter sensitivity of the DRSTI Model.

Parameters	Theoretical Weighting	Theoretical Weighting (%)	Effective Weighting (%)			
			Average	Minimum	Maximum	Standard Deviation
D	5	29.41	28.85	23.44	31.25	32.27
R	4	23.53	32.69	50	25	7.07
S	2	11.76	8.85	3.13	12.50	15.25
T	1	5.88	5.38	1.56	6.94	9.62
I	5	29.41	27.47	15.63	31.25	32.04

　　　　The verification of model validation of groundwater vulnerability assessment relative to potentially toxic elements contamination associated with the historical exploitation of the Ouixane mining district was also carried out by comparing the values of groundwater electrical conductivity (EC) and (S) concentration in different sites, with the vulnerability index (Vi) values of the corresponding sites. The obtained results show a significant correlation (Figure 15a,b). An increase in the Vi value will correspond to an increase in groundwater EC and S concentration. So, the sites with a medium to high vulnerability

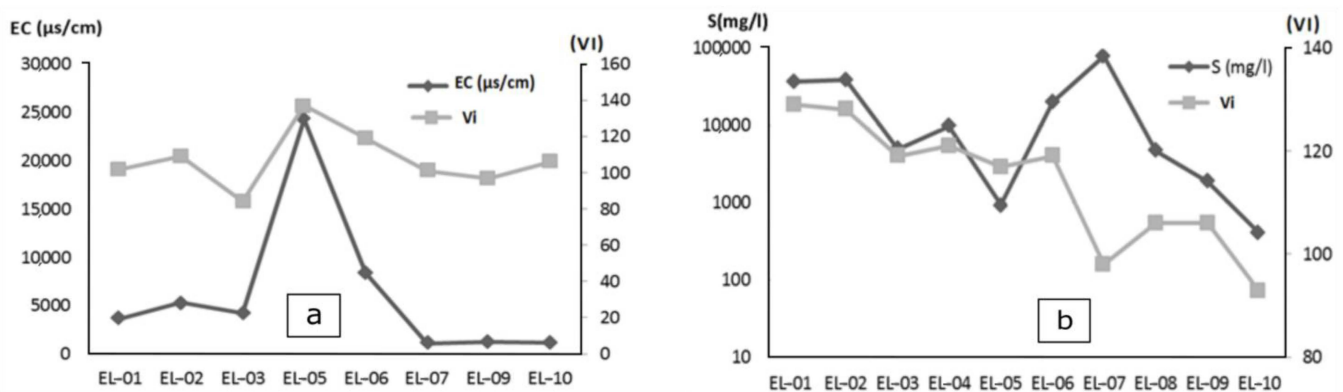correspond to areas contaminated by potentially toxic elements associated with the mining site of Ouixane.

Figure 15. Relation between groundwater electric conductivity (EC) (**a**), groundwater sulfur (S) concentration (**b**), and the vulnerability index values from the Ouixane area.

4.2. Groundwater Vulnerability Risk

In this methodology, groundwater risk assessment includes all activities that constitute possible origins of potentially toxic elements contamination. The potential release points of mining contamination (waste rock and tailings) are normally enriched in potentially toxic elements and sulfides [4,9]. A groundwater risk map will be obtained considering the spatial distribution of toxic elements pollution sources and the probability of its release [51], by overlaying the vulnerability map and the map of mining tailings (Figure 16) potentially emitting metallic pollution.

The delimitation of areas of groundwater contamination risk, in the Ouixane mining district, showed three classes of risk: high, medium, and low.

The overlay results showed that 90% of the mining discharges are deposited in areas with high to medium groundwater vulnerability, which represent medium to high-risk areas. The obtained results demonstrate that anthropogenic activities play a crucial role in the environmental contamination risk increase, and the risk is all the greater when the sources of contamination, represented by tailing and waste rocks, are close to vulnerable areas, which can compromise the sustainability of groundwater resources.

The presence on the surface of waste rock and tailings rich in alterable minerals (sulfides and iron oxides), increases the mechanisms of toxic elements transfer to groundwater, promoting the production of AMD since mitigation measures will not be considered urgently. In addition, the existence of ferric iron in tailings induces the oxidation of other sulfides, reactivating the release of metals (e.g., As, Cu, Cr, Cd, Pb, Zn, Ni), which could exceed several times their content in the initial ore. This is the case of Cr, As, Cd, Cu, and S groundwater contents, which probably are associated with the alteration of waste rock, containing arsenopyrite, chalcopyrite, galena, and sphalerite [52,53].

Rehabilitation, mitigation, and/or remediation strategy and actions plan should be implemented according to the degree of contamination, by prioritizing the most contaminated sites (Figure 16) given that the budgets allocated to such actions are onerous. Thus, the rehabilitation and mitigation strategy and actions are not enough without setting up an environmental monitoring and control system to ensure the efficiency of the envisaged measures, especially for acid mine drainage monitoring, which should be composed of a network of piezometers for qualitative (heavy metal concentration, physicochemical and biological parameters, etc.) and quantitative (piezometric level, static and dynamic level, drawdown, storage coefficient, etc.) monitoring of water resources in the Ouixane mining environment.
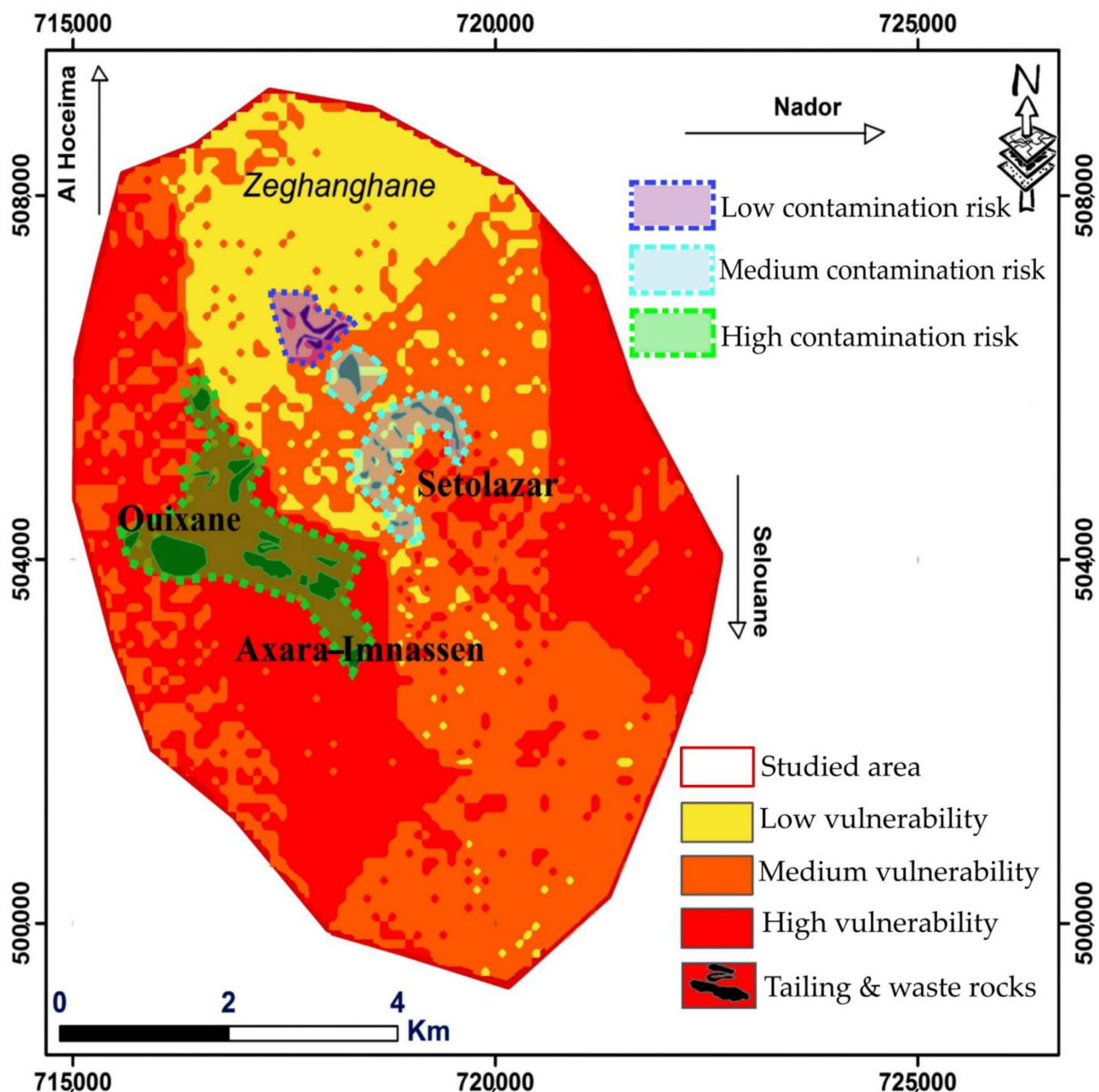
Figure 16. Spatial distribution of tailings on the groundwater intrinsic vulnerability map.

5. Conclusions

The groundwater vulnerability map allows the identification of the most exposed areas to groundwater potentially toxic elements. The potential vulnerability map of the aquifer shows that the main part of the studied area is covered by a medium groundwater vulnerability zone, followed by high groundwater vulnerability areas. However, the parameters that significantly influenced the groundwater vulnerability assessment correspond to the water depth (D), the unsaturated zone (I), and the net recharge (R).

The contribution of the application of the method used regarding the management strategies in a water-deficient area resides in the:

(1) Mapping of vulnerability zones, which is a decisive tool for identifying priority areas for intervention;

(2) Study of the spatial distribution of the pollution sources (such as heavy metal contamination) on the one hand, and of the vulnerability zones on the other, which is decisive for the identification of high-risk contamination sites and therefore supports the management of mining waters pollution risks;

(3)   Identification of parameters involving vulnerability, which are crucial for a targeted intervention on these parameters to control the spread of mining contamination.

References

1. Wang, X.; Cui, L.; Li, J.; Zhang, C.; Gao, X.; Fan, B.; Liu, Z. Water quality criteria for the protection of human health of 15 toxic metals and their human risk in surface water, China. *Environ. Pollut.* **2021**, *276*, 116628. [CrossRef] [PubMed]
2. Guo, X.X.; Liu, H.T.; Zhang, J. The role of biochar in organic waste composting and soil improvement: A review. *Waste Manag.* **2020**, *102*, 884–899. [CrossRef] [PubMed]
3. Khafouri, A.; Talbi, E.H.; Abdelouas, A. Assessment of Heavy Metal Contamination of the Environment in the Mining Site of Ouixane (North East Morocco). *Water Air Soil Pollut.* **2021**, *232*, 398. [CrossRef]
4. Jabrane, R. Etudes Génétiques de la Minéralisation en fer de Nador (Maroc Nord Oriental). Ph.D. Dissertation, Université Libre de Bruxelles, Bruxelles, Belgium, 1993.
5. Kerchaoui, S. Etude Géologique et Structurale du Massif des Beni Bou Ifrour (Rif Oriental, Maroc). Ph.D. Dissertation, Université de Paris-Sud, Paris, France, 1985.
6. Chamrar, A.; Oujidi, M.; El Mandour, A.; Jilali, A. 3D geological modeling of Gareb-Bouareg basin in northeast Morocco. *J. Afr. Earth Sci.* **2019**, *154*, 172–180. [CrossRef]
7. Rhazi, M.E.; Hayashi, K.I. Mineralogy, geochemistry, and age constraints on the Beni Bou Ifrour skarn type magnetite deposit, northeastern Morocco. *Resour. Geol.* **2002**, *52*, 25–39. [CrossRef]
8. Lebret, N. Contexte Structural et Métallogénique des Skarns à Magnétite des Beni Bou Ifrour (Rif Oriental, Maroc). Apports à L'évolution Géodynamique de la Méditerranée occidentale. Ph.D. Dissertation, Université d'Orléans, Orléans, France, 2014.
9. Lakrim, M.; Mesrar, L.; El Aroussi, O.; Lahrach, A.; Beaabidate, L.; Garouani, A.; Chaouni, A.; Tabyaoui, H.; Jabrane, R. Impact study of Mining waste of The Nador mine on the Environment (North-Eastern of Morocco). *Revue LJEE* **2011**, *18*, 78–94.
10. Bouabdellah, M.; Jabrane, R.; Margoum, D.; Sadequi, M. Skarn to Porphyry-Epithermal Transition in the Ouixane Fe District, Northeast Morocco: Interplay of Meteoric Water and Magmatic-Hydrothermal Fluids. In *Mineral Deposits of North Africa*; Bouabdellah, M., Slack, J., Eds.; Springer: Cham, Switzerland, 2016. [CrossRef]
11. Benidire, L.; Pereira, S.I.A.; Loqman, S.; Castro, P.M.L.; Boularbah, A. Physical, Chemical, and Microbiological Characterization of Kettara Mine Tailings, Morocco. *Soil Syst.* **2022**, *6*, 23. [CrossRef]
12. Azzeddine, K.; El Hassan, T. Assessment of Metallic Contamination of Water Resources in the Area around the Abandoned Mining Site of Ouixane (North East Morocco). In Proceedings of the 4th Edition of International Conference on Geo-IT and Water Resources 2020, Al-Hoceima, Morocco, 11–12 March 2020; pp. 1–6.
13. Fang, Z.; Liu, Z.; Zhao, S.; Ma, Y.; Li, X.; Gao, H. Assessment of Groundwater Contamination Risk in Oilfield Drilling Sites Based on Groundwater Vulnerability, Pollution Source Hazard, and Groundwater Value Function in Yitong County. *Water* **2022**, *14*, 628. [CrossRef]
14. El Rhazi, M. Mineralogy, Geochemistry, and Age Constraints on the Beni Bou Ifrour Skarn Type Magnetite Deposit, Northeastern Morocco. Ph.D. Dissertation, Tohoku University, Sendai, Japan, 2002.
15. Lyazidi, R.; Hessane, M.A.; Moutei, J.F.; Bahir, M.; Ouhamdouch, S. Management of water resource from semi arid area by elaborating database under GIS: Case of Gareb-Bouareg aquifer (Rif, Morocco). *Arab. J. Geosci.* **2019**, *12*, 352. [CrossRef]
16. El Yaouti, F.; El Mandour, A.; Khattach, D.; Benavente, J.; Kaufmann, O. Salinization processes in the unconfined aquifer of Bou-Areg (NE Morocco): A geostatistical, geochemical, and tomographic study. *Appl. Geochem.* **2009**, *24*, 16–31. [CrossRef]
17. Nguyen, T.T.; Ngo, H.H.; Guo, W.; Nguyen, H.Q.; Luu, C.; Dang, K.B.; Liu, Y.; Zhang, X. New approach of water quantity vulnerability assessment using satellite images and GIS-based model: An application to a case study in Vietnam. *Sci. Total Environ.* **2020**, *737*, 139784. [CrossRef] [PubMed]

18. Knouz, N.; Boudhar, A.; Bachaoui, E.M.; Saadi, C. Comparative approach of three popular intrinsic vulnerability methods: Case of the Beni Amir groundwater (Morocco). *Arab. J. Geosci.* **2018**, *11*, 281. [CrossRef]

19. Aller, L.; Bennett, T.; Lehr, J.; Petty, R.J.; Hackett, G. *DRASTIC: A Standardized System for Evaluating Groundwater Pollution Potential Using Hydrogeologic Settings*; US Environmental Protection Agency: Washington, DC, USA, 1987; 455p.

20. Benjmel, K.; Amraoui, F.; Aydda, A.; Tahiri, A.; Yousif, M.; Pradhan, B.; Abdelrahman, K.; Fnais, M.S.; Abioui, M. A multidisciplinary approach for groundwater potential mapping in a fractured semi-arid terrain (Kerdous Inlier, Western Anti-Atlas, Morocco). *Water* **2022**, *14*, 1553. [CrossRef]

21. Gonçalves, V.; Albuquerque, A.; Almeida, P.G.; Cavaleiro, V. DRASTIC Index GIS-Based Vulnerability Map for the Entre-os-Rios Thermal Aquifer. *Water* **2022**, *14*, 2448. [CrossRef]

22. Machiwal, D.; Jha, M.K.; Singh, V.P.; Mohan, C. Assessment and mapping of groundwater vulnerability to pollution: Current status and challenges. *Earth-Sci. Rev.* **2018**, *185*, 901–927. [CrossRef]

23. Li, R.; Merchant, J.W. Modeling vulnerability of groundwater to pollution under future scenarios of climate change and biofuels-related land use change: A case study in North Dakota, USA. *Sci. Total Environ.* **2013**, *447*, 32–45. [CrossRef]

24. Wang, J.; He, J.; Chen, H. Assessment of groundwater contamination risk using hazard quantification, a modified DRASTIC model and groundwater value, Beijing Plain, China. *Sci. Total Environ.* **2012**, *432*, 216–226. [CrossRef]

25. Barbulescu, A. Assessing groundwater vulnerability: DRASTIC and DRASTIC-like methods: A review. *Water* **2020**, *12*, 1356. [CrossRef]

26. El Hmaidi, A.; Talhaoui, A.; Manssouri, I.; Jaddi, H.; Ben-Daoud, M.; Kasse, Z.; El Ouali, A.; Essahlaoui, A. Assessment of the physicochemical water quality of the Moulouya River, Morocco, using the SEQ-Eau index. *Environ. Monit. Assess.* **2022**, *194*, 37. [CrossRef]

27. Hasan, M.; Islam, M.A.; Hasan, M.A.; Alam, M.J.; Peas, M.H. Groundwater vulnerability assessment in Savarupazila of Dhaka district, Bangladesh—A GIS-based DRASTIC modeling. *Groundw. Sustain. Dev.* **2019**, *9*, 100220. [CrossRef]

28. Aslam, R.A.; Shrestha, S.; Pandey, V.P. Groundwater vulnerability to climate change: A review of the assessment methodology. *Sci. Total Environ.* **2018**, *612*, 853–875. [CrossRef] [PubMed]

29. Aswathi, J.; Sajinkumar, K.S.; Rajaneesh, A.; Oommen, T.; Bouali, E.H.; Binojkumar, R.B.; Rani, V.R.; Thomas, J.; Thrivikramji, K.P.; Ajin, R.S.; et al. Furthering the precision of RUSLE soil erosion with PSInSAR data: An innovative model. *Geocarto Int.* **2022**, 1–22. [CrossRef]

30. Thapa, R.; Mirsky, S.B.; Tully, K.L. Cover crops reduce nitrate leaching in agroecosystems: A global meta-analysis. *J. Environ. Qual.* **2018**, *47*, 1400–1411. [CrossRef] [PubMed]

31. Shirazi, S.M.; Imran, H.M.; Akib, S. GIS-based DRASTIC method for groundwater vulnerability assessment: A review. *J. Risk Res.* **2012**, *15*, 991–1011. [CrossRef]

32. Asfaw, D.; Mengistu, D. Modeling megech watershed aquifer vulnerability to pollution using modified DRASTIC model for sustainable groundwater management, Northwestern Ethiopia. *Groundw. Sustain. Dev.* **2020**, *11*, 100375. [CrossRef]

33. Malakootian, M.; Nozari, M. GIS-based DRASTIC and composite DRASTIC indices for assessing groundwater vulnerability in the Baghin aquifer, Kerman, Iran. *Nat. Hazards Earth Syst. Sci.* **2020**, *20*, 2351–2363. [CrossRef]

34. Wu, X.; Li, B.; Ma, C. Assessment of groundwater vulnerability by applying the modified DRASTIC model in Beihai City, China. *Environ. Sci. Pollut. Res.* **2018**, *25*, 12713–12727. [CrossRef]

35. Babiker, I.S.; Mohamed, M.A.; Hiyama, T.; Kato, K. A GIS-based DRASTIC model for assessing aquifer vulnerability in Kakamigahara Heights, Gifu Prefecture, central Japan. *Sci. Total Environ.* **2005**, *345*, 127–140. [CrossRef]

36. Tiwari, A.K.; Singh, P.K.; De Maio, M. Evaluation of aquifer vulnerability in a coal mining of India by using GIS-based DRASTIC model. *Arab. J. Geosci.* **2016**, *9*, 438. [CrossRef]

37. Sidibe, A.M.; Xueyu, L. Heavy metals and nitrate to validate groundwater sensibility assessment based on DRASTIC models and GIS: Case of the upper Niger and the Bani basin in Mali. *J. Afr. Earth Sci.* **2018**, *147*, 199–210. [CrossRef]

38. Jang, W.S.; Engel, B.; Harbor, J.; Theller, L. Aquifer vulnerability assessment for sustainable groundwater management using DRASTIC. *Water* **2017**, *9*, 792. [CrossRef]

39. Kostyuchenko, Y.; Artemenko, I.; Abioui, M.; Benssaou, M. Global and Regional Climatic Modeling. In *Encyclopedia of Mathematical Geosciences*; DayaSagar, B., Cheng, Q., McKinley, J., Agterberg, F., Eds.; Springer: Cham, Switzerland, 2022. [CrossRef]

40. Tekken, V.; Kropp, J.P. Climate-Driven or Human-Induced: Indicating Severe Water Scarcity in the Moulouya River Basin (Morocco). *Water* **2012**, *4*, 959–982. [CrossRef]

41. Chitsazan, M.; Akhtari, Y. A GIS-based DRASTIC model for assessing aquifer vulnerability in Kherran Plain, Khuzestan, Iran. *Water Resour. Manag.* **2009**, *23*, 1137–1155. [CrossRef]

42. Chaturvedi, M.C.; Srivastava, V.K. Induced groundwater recharge in the Ganges basin. *Water Resour. Res.* **1979**, *15*, 1156–1166. [CrossRef]

43. Al-Abadi, A.M.; Al-Shamma'a, A.M.; Aljabbari, M.H. A GIS-based DRASTIC model for assessing intrinsic groundwater vulnerability in northeastern Missan governorate, southern Iraq. *Appl. Water Sci.* **2017**, *7*, 89–101. [CrossRef]

44. Kazakis, N.; Voudouris, K.S. Groundwater vulnerability and pollution risk assessment of porous aquifers to nitrate: Modifying the DRASTIC method using quantitative parameters. *J. Hydrol.* **2015**, *525*, 13–25. [CrossRef]

45. Souleymane, K.; Zhonghua, T. A novel method of sensitivity analysis testing by applying the DRASTIC and fuzzy optimization methods to assess groundwater vulnerability to pollution: The case of the Senegal River basin in Mali. *Nat. Hazards Earth Syst. Sci.* **2017**, *17*, 1375–1392. [CrossRef]

46. Atiqur, R. A GIS based DRASTIC model for assessing groundwater vulnerability in shallow aquifer in Aligarh, India. *Appl. Geogr.* **2008**, *28*, 32–53. [CrossRef]

47. Le, T.N.; Tran, D.X.; Tran, T.V.; Gyeltshen, S.; Lam, T.V.; Luu, T.H.; Nguyen, D.Q.; Dao, T.V. Estimating Soil Water Susceptibility to Salinization in the Mekong River Delta Using a Modified DRASTIC Model. *Water* **2021**, *13*, 1636. [CrossRef]

48. Baghapour, M.A.; Fadaei Nobandegani, A.; Talebbeydokhti, N.; Bagherzadeh, S.; Nadiri, A.A.; Gharekhani, M.; Chitsazan, N. Optimization of DRASTIC method by artificial neural network, nitrate vulnerability index, and composite DRASTIC models to assess groundwater vulnerability for unconfined aquifer of Shiraz Plain, Iran. *J. Environ. Health Sci. Eng.* **2016**, *14*, 13. [CrossRef]

49. Abiy, A.Z.; Melesse, A.M. Evaluation of watershed scale changes in groundwater and soil moisture storage with the application of GRACE satellite imagery data. *Catena* **2017**, *153*, 50–60. [CrossRef]

50. Witkowski, A.J. Groundwater vulnerability: From scientific concept to practical application. *Environ. Earth Sci.* **2016**, *75*, 1134. [CrossRef]

51. Abera, K.A.; Gebreyohannes, T.; Abrha, B.; Hagos, M.; Berhane, G.; Hussien, A.; Belay, A.S.; Van Camp, M.; Walraevens, K. Vulnerability Mapping of Groundwater Resources of Mekelle City and Surroundings, Tigray Region, Ethiopia. *Water* **2022**, *14*, 2577. [CrossRef]

52. Lghoul, M.; Maqsoud, A.; Hakkou, R.; Kchikach, A. Hydrogeochemical behavior around the abandoned Kettara mine site, Morocco. *J. Geochem. Explor.* **2014**, *144*, 456–467. [CrossRef]

53. Mabroum, S.; Moukannaa, S.; El Machi, A.; Taha, Y.; Benzaazoua, M.; Hakkou, R. Mine wastes based geopolymers: A critical review. *Clean. Eng. Technol.* **2020**, *1*, 100014. [CrossRef]